Inertial Lubrication Theory

N. O. Rojas,[1] M. Argentina,[1] E. Cerda,[2] and E. Tirapegui[3]

[1]*Université de Nice Sophia Antipolis, Laboratoire J. A. Dieudonné, Parc Valrose, 06108 Nice Cedex 2, France*
[2]*Departamento de Física, Universidad de Santiago, Av. Ecuador 3493, Santiago, Chile*
[3]*Departamento de Física, Universidad de Chile, Facultad de Ciencias Físicas y Matemáticas, Av. Blanco Encalada 2008, Santiago, Chile*

(Received 8 September 2009; published 7 May 2010)

Thin fluid films can have surprising behavior depending on the boundary conditions enforced, the energy input and the specific Reynolds number of the fluid motion. Here we study the equations of motion for a thin fluid film with a free boundary and its other interface in contact with a solid wall. Although shear dissipation increases for thinner layers and the motion can generally be described in the limit as viscous, inertial modes can always be excited for a sufficiently high input of energy. We derive the minimal set of equations containing inertial effects in this strongly dissipative regime.

DOI: 10.1103/PhysRevLett.104.187801 PACS numbers: 68.15.+e, 47.10.ad, 47.20.Ky, 47.55.nd

When the smaller length scale in a fluid layer is its thickness a depth average version of the Navier-Stokes (NS) equations is much expected. The well-known shallow water equations [1,2] describing the motion of a fluid layer at high Reynolds numbers is the classic example provided in fluid mechanics textbooks. Their simplicity and tractability allow for explaining phenomena such as wave propagation, hydraulic jumps or shock waves. In the opposite low Reynolds number regime, several authors have explored the buckling behavior of viscous films bounded by free surfaces. The elasticlike response of a fluid, primarily established as a formal analogy by Stokes and Rayleigh more than a century ago [3], has been explained by deriving from the NS equations the equivalent of the Föpl–Von Kármán equations in elastic plate theory [4,5]. These equations at the leading order show the constancy of the layer thickness and a faster motion in the out-of-plane direction than the motion in the plane of the film.

When one of the boundaries is in contact with a solid wall, the behavior of a viscous fluid sheet changes dramatically. The free film lubrication theory [2,6] takes account of this condition. The no-slip condition at one boundary implies that shear plays a role and dissipation is much more effective. The in-plane motion is now faster than the motion perpendicular to the film, and the film thickness changes with the position of the free boundary. In this highly dissipative condition, the dynamics of the fluid film is obtained from the quasistatic balance between viscous forces and external forces like gravity, surface tension or an imposed pressure gradient. Thus, the inertial terms in the NS equations do not play any role in the motion of the fluid at this level of approximation.

There are, however, physical situations in which the inertial modes are necessary to inject energy into the system. The circular hydraulic jump observed in viscous fluid films [7–9] is explained as a singularity line spatially connecting a state where inertial modes are dominant versus a state where the film is in a lubrication regime. A different example is given by Faraday waves [10], observed when a viscous fluid film is vertically and periodically accelerated, which cannot be explained by lubrication theory alone; inertial terms have to be included in the linear analysis of the NS equations to capture the instability [11,12]. There is no known systematic derivation of the effective nonlinear equations describing the behavior of a thin fluid film under the aforementioned conditions, although a depth averaging of the NS equations could be expected to lead to such approximation. Here we find these equations and apply them in these two cases. We show that they contain the physics of the hydraulic jump and can be used to explain the radius separating the inertial and viscous regimes. We also show how these equations explain the creation and saturation of the patterns observed in the case of Faraday instability.

We consider a rigid plate covered by a thin fluid layer embedded in a system with horizontal and vertical coordinates $\mathbf{x} = (x, y)$, z respectively. The velocity field is $\mathbf{v}(\mathbf{x}, z, t)$, where $z = 0$ is the position of the plate and $z = h$ corresponds to the fluid at rest. The basic configuration is the rest state $\mathbf{v}(\mathbf{x}, z, t) = 0$ with a flat interface and a hydrostatic pressure $p_s = p_0 - \rho g[z - h]$, where p_0 is the atmospheric pressure, ρ the mass density of the fluid and g is gravity. The incompressible Navier-Stokes equations are [1,2]:

$$\partial_t \mathbf{v} + (\mathbf{v} \cdot \nabla)\mathbf{v} = -\nabla \pi + \nu \nabla^2 \mathbf{v} \text{ and } \nabla \cdot \mathbf{v} = 0, \quad (1)$$

where ν is the kinematic viscosity of the fluid and $\pi = (p - p_s)/\rho$ is related to the deviation of the pressure field $p(\mathbf{x}, z, t)$ from the hydrostatic pressure. The kinematic condition at $z = \xi(\mathbf{x}, t)$ is $v_z|_{z=\xi} = \partial_t \xi + (\mathbf{v}_\perp|_{z=\xi} \cdot \nabla_\perp)\xi$. This condition in combination with the no-slip boundary condition on the bottom wall gives the conservation law

$$\partial_t \xi + \nabla_\perp \cdot \mathbf{q} = 0, \tag{2}$$

$$\mathbf{q}(\mathbf{x}, t) = \int_0^\xi \mathbf{v}_\perp(\mathbf{x}, z, t) dz, \tag{3}$$

where $\mathbf{v}_\perp(\mathbf{x}, z, t)$ and $\nabla_\perp = (\partial_x, \partial_y)$ are the horizontal velocity field and the horizontal gradient, respectively, and $\mathbf{q}$ is the horizontal flux. Motivated by the standard lubrication theory [2,6], we aim to find a set of equations involving just the amplitude ξ and the flux $\mathbf{q}$; thus, the conservation law (2) constitutes the first equation of the set.

The continuity of the stress across the free surface is $T_{jk}\hat{n}_k|_{z=\xi} = [p_0 + \gamma\kappa]\hat{n}_j$ where T_{jk} is the usual stress tensor [1], $\hat{n}$ is the normal unitary vector at the free surface, γ is the surface tension, and $\kappa = -\nabla_\perp^2 \xi/(\sqrt{1 + (\nabla_\perp \xi)^2})^3$ is the mean curvature of the surface. The no-slip boundary condition on the plate is $\mathbf{v}(\mathbf{x}, z, t)|_{z=0} = 0$. We will ignore lateral boundary conditions since, for a highly viscous fluid and large aspect ratio, they have no influence [13].

In order to render these equations dimensionless, we scale all the variables. The horizontal coordinates are scaled with a characteristic horizontal length L as $(\tilde{x}, \tilde{y}) = (x, y)/L$ and the vertical coordinates are naturally scaled with the height of the fluid as $(\tilde{z}, \tilde{\xi}) = (z, \xi)/h$, where the tilde denotes dimensionless quantities. For the velocities, the scaling is $(\tilde{v}_x, \tilde{v}_y) = \mathbf{v}_\perp/\Omega L$ and $\tilde{v}_z = v_z/\Omega h$, where Ω is a characteristic frequency of energy injection in the system. Hence, the new time, $\tilde{t}$, and pressure, $\tilde{\pi}$, are $\tilde{t} = \Omega t$ and $\tilde{\pi} = h^2\pi/\nu\Omega L^2$.

Substitution of these scaling into the bulk equations and boundary conditions yields: (The tilde notation is henceforth dropped.)

$$\begin{aligned} &\mathrm{Re}[\partial_t + (\mathbf{v}\cdot\nabla)]\mathbf{v}_\perp = -\nabla_\perp \pi + (\epsilon^2\nabla_\perp^2 + \partial_z^2)\mathbf{v}_\perp, \\ &\epsilon^2\mathrm{Re}[\partial_t + (\mathbf{v}\cdot\nabla)]v_z = -\partial_z \pi + \epsilon^2(\epsilon^2\nabla_\perp^2 + \partial_z^2)v_z, \end{aligned} \tag{4}$$

where the slenderness ratio $\epsilon = h/L$ characterizes the thickness of the sheet to L and $\mathrm{Re} = \Omega h^2/\nu$ is the Reynolds number. For very thin films $\epsilon \ll 1$, the continuity of the stress in the tangential direction gives

$$\partial_z \mathbf{v}_\perp|_{z=\xi} + \epsilon^2 \mathbf{A} + \mathcal{O}(\epsilon^4) = 0 \tag{5}$$

where $\mathbf{A} = \{\nabla_\perp v_z + (\nabla_\perp \xi \cdot \partial_z \mathbf{v}_\perp)\nabla_\perp \xi - \nabla_\perp(\nabla_\perp \xi \cdot \mathbf{v}_\perp) + [\mathbf{v}_\perp, \nabla_\perp \xi]\}_{z=\xi} - 2\nabla_\perp \xi\{\nabla_\perp \cdot (\mathbf{v}_\perp|_{z=\xi})\}$, and $[\cdots]$ is the Lie bracket $[\mathbf{a}, \mathbf{b}] = (\mathbf{a}\cdot\nabla)\mathbf{b} - (\mathbf{b}\cdot\nabla)\mathbf{a}$. For the normal component, the continuity of the stress yields

$$\pi|_{z=\xi} + 2\epsilon^2 \nabla_\perp \cdot (\mathbf{v}_\perp|_{z=\xi}) = G[\xi - 1] - B\nabla_\perp^2 \xi + \mathcal{O}(\epsilon^4), \tag{6}$$

where $G = gh^3/\nu\Omega L^2$ and $B = \gamma h^3/\rho\nu\Omega L^4$. These scalings leave invariant the incompressibility relation, the conservation law (2) and (3) and the no-slip boundary condition.

In order to develop the nonlinear equation for the interfacial disturbance $\xi(\mathbf{x}, t)$ and the lateral flux $\mathbf{q}(\mathbf{x}, t)$, we need further approximations. Starting from the definition of boundary layer $\delta = \sqrt{\nu/\Omega}$ [1], and assuming that thickness is the smaller length scale in the system, we conclude that $h \ll \delta$ or $\mathrm{Re} \ll 1$. Thus, we have two expansion parameters, ϵ^2 and Re, that we will study at the lowest order by neglecting $\mathcal{O}(\epsilon^4, \epsilon^2\mathrm{Re}, \mathrm{Re}^2, \ldots)$ terms. Since the fluid layer is thin, we perform a Taylor expansion on the variable z where the incompressibility relation and the no-slip boundary condition on the plate has been used to get the relations $\mathbf{v}_\perp(\mathbf{x}, z, t) = \sum_{n=0}^\infty \mathbf{v}_n(\mathbf{x}, t)\frac{z^{n+1}}{(n+1)!}$, $v_z(\mathbf{x}, z, t) = -\sum_{n=0}^\infty \nabla_\perp \cdot \mathbf{v}_n(\mathbf{x}, t)\frac{z^{n+2}}{(n+2)!}$, and $\pi(\mathbf{x}, z, t) = \sum_{n=0}^\infty \pi_n(\mathbf{x}, t)\frac{z^n}{n!}$. Replacing these expansions into (4) and solving for each order we get at first order in ϵ^2 and Re:

$$\begin{aligned} &\pi_1 = -\epsilon^2 \nabla_\perp \cdot \mathbf{v}_0, \qquad \pi_2 = -\epsilon^2 \nabla_\perp^2 \pi_0, \qquad \pi_3 = \mathcal{O}(\epsilon^4) \\ &\mathbf{v}_1 = \nabla_\perp \pi_0, \qquad \mathbf{v}_2 = \mathrm{Re}\partial_t \mathbf{v}_0 - \epsilon^2[\nabla_\perp^2 \mathbf{v}_0 + \nabla_\perp(\nabla_\perp \cdot \mathbf{v}_0)], \\ &\mathbf{v}_3 = \mathrm{Re}[\partial_t \nabla_\perp \pi_0 + 2(\mathbf{v}_0 \cdot \nabla_\perp)\mathbf{v}_0 - \mathbf{v}_0(\nabla_\perp \cdot \mathbf{v}_0)] \\ &\qquad - 2\epsilon^2 \nabla^2(\nabla_\perp \pi_0), \\ &\mathbf{v}_4 = \mathrm{Re}[3(\nabla_\perp \pi_0 \cdot \nabla_\perp)\mathbf{v}_0 - 3(\nabla_\perp \cdot \mathbf{v}_0)\nabla_\perp \pi_0 \\ &\qquad + 3(\mathbf{v}_0 \cdot \nabla_\perp)\nabla_\perp \pi_0 - \mathbf{v}_0(\nabla_\perp^2 \pi_0)] + \mathcal{O}(\epsilon^4, \epsilon^2\mathrm{Re}, \mathrm{Re}^2), \\ &\mathbf{v}_5 = \mathrm{Re}[-4\nabla_\perp \pi_0(\nabla_\perp^2 \pi_0) + 6(\nabla_\perp \pi_0 \cdot \nabla_\perp)\nabla_\perp \pi_0] \\ &\qquad + \mathcal{O}(\epsilon^4, \epsilon^2\mathrm{Re}, \mathrm{Re}^2) \qquad \mathbf{v}_6 = \mathcal{O}(\epsilon^4, \epsilon^2\mathrm{Re}, \mathrm{Re}^2). \end{aligned} \tag{7}$$

The other remaining functions are neglected at order $\mathcal{O}(\epsilon^4, \epsilon^2\mathrm{Re}, \mathrm{Re}^2, \ldots)$. Our strategy to obtain the dynamic equation connecting the flux $\mathbf{q}$ and ξ is the following: First, the last two unknowns $\mathbf{v}_0$ and π_0 can be computed in terms of the lateral flux $\mathbf{q}$ and the surface profile ξ by solving Eq. (3) and the surface condition (5). Second, by replacing these functions into (6) we obtain a dynamic equation for $\mathbf{q}$ and ξ that, with Eq. (2), completes our set of equations for the fluid film. [See supplementary material [14] for a detailed description of the inversion process and evaluation of Eq. (6).] At the lowest order in the parameters ϵ^2 and Re, we obtain

$$\begin{aligned} &\partial_t \xi + \nabla_\perp \cdot \mathbf{q} = 0, \\ &\mathrm{Re}\mathcal{E}(\xi, \mathbf{q}) + \epsilon^2 \mathcal{F}(\xi, \mathbf{q}) + 3\mathbf{q} + \xi^3(G - B\nabla_\perp^2)\nabla_\perp \xi = 0. \end{aligned} \tag{8}$$

Here

$$\begin{aligned} \mathcal{E} &= \frac{6}{5}\left[\left(\xi^3\partial_t + \frac{9}{7}\xi^2(\mathbf{q}\cdot\nabla_\perp)\right)\left(\frac{\mathbf{q}}{\xi}\right) + \frac{1}{7}\xi\mathbf{q}(\nabla_\perp \cdot \mathbf{q})\right] \\ \mathcal{F} &= -\frac{3}{2}\left[-\xi^2\mathbf{A} + \xi^3\nabla_\perp\left\{\nabla_\perp \cdot \left(\frac{\mathbf{q}}{\xi}\right)\right\} + \frac{5}{4}\xi^4\left\{\nabla_\perp^2\left(\frac{\mathbf{q}}{\xi^2}\right)\right.\right. \\ &\quad \left.\left. + \nabla_\perp\left[\nabla_\perp \cdot \left(\frac{\mathbf{q}}{\xi^2}\right)\right]\right\} - \frac{9}{10}\xi^5\nabla_\perp^2\left(\frac{\mathbf{q}}{\xi^3}\right)\right] \end{aligned}$$

where $\mathbf{A}$ is after the inversion process $\mathbf{A} = -\nabla_\perp(\nabla_\perp \cdot \mathbf{q}) + \frac{3}{2}[\frac{\mathbf{q}}{\xi}, \nabla_\perp \xi] - \frac{3}{2}\nabla_\perp \xi[\nabla_\perp \cdot (\frac{\mathbf{q}}{\xi})]$. Note that in the extremely viscous ($\mathrm{Re} \to 0$) and shallow water limit ($\epsilon^2 \to 0$), Eqs. (8) reduces to the Reynolds lubrication equation [6] $\partial_t \xi = \frac{1}{3}\nabla_\perp \cdot [\xi^3\{(G - B\nabla_\perp^2)\nabla_\perp \xi\}]$.

As a first application, our equations can be used to study the steady state flow observed in circular hydraulic jumps (see Fig. 1). We observe that the conservation law is now $\nabla_\perp \cdot \mathbf{q} = 0$ which can be solved using cylindrical coordinates for the axisymmetric case as $\mathbf{q} = q(r)\hat{r}$, where $q(r) = Q/2\pi r$ and Q is a dimensionless constant. In terms of our unscaled variables $Q = Q_0/(\Omega h_c R_c^2)$ where Q_0 is the total volume of fluid per unit of time injected at the center of the system. Inspired by the experiments of Hansen *et al.* [9], we take L as the radius of the circular container, R_c, and h as the height of the fluid layer in its perimeter, h_c (see Fig. 1). It gives $\epsilon = h_c/R_c$. The total kinetic energy in the system is proportional to the volume of fluid in the container $V \sim \pi R_c^2 h_c$ so that the time scale for injection of new energy into the system is of the order $\Omega^{-1} = V/Q_0$. Thus, the characteristic frequency is $\Omega = Q_0/(\pi R_c^2 h_c)$. It gives a Reynolds number $\mathrm{Re} = Q_0 h_c/(\pi R_c^2 \nu)$. A straightforward calculation from the second of Eqs. (8) yields

$$\frac{54\mathrm{Re}}{35} q(q'\xi - q\xi') + \frac{3\epsilon^2}{10}(24q\xi\xi'' + 9q'\xi\xi' - 16q\xi'^2) + 3q + \xi^3[G\xi' - B(\xi''' + \xi''/r - \xi'/r^2)] = 0. \quad (9)$$

Here $(\cdots)' = d(\cdots)/dr$. We numerically compute the solution to this equation by using a standard Runge-Kutta method with the boundary conditions $\xi(1) = 1$, and $\xi'(1) = \xi''(1) = 0$. The last two boundary conditions enforce a flat horizontal profile at the boundary of the container as observed in the experiments. Figure 1 shows the profile computed from Eq. (9) for a set of experimental parameters obtained from Ref. [7]. It contains one region of high velocity where the fluid layer is shallow and a slower region where the height of the fluid is of the order $\mathcal{O}(1)$. Both regions are connected by a narrow region where there is a sharp variation in the height defining the radius of the hydraulic jump r_j. More precisely, we define this radius as the point where a change of curvature is detected from being positive in the faster region to being negative in the slower region [$\xi''(r_j) = 0$ at that point].

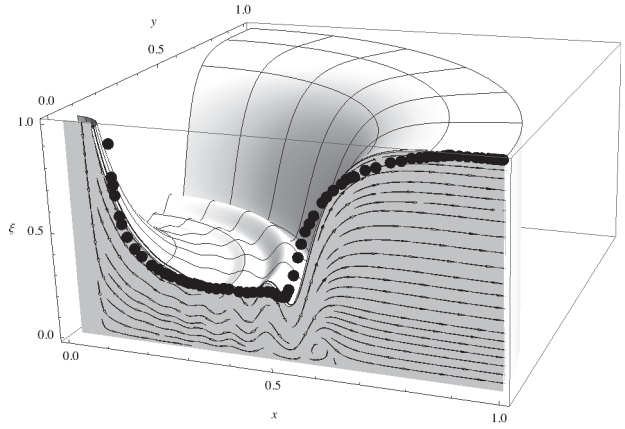

FIG. 1. 3D view of a circular hydraulic jump in dimensionless coordinates obtained using the inertial lubrication theory. On the plane $y = 0$, we represent the profile of the film thickness ξ and the streamlines of the fluid. The black dots are experimental measures of the surface profile extracted from Ref. [7]. Here the fluid is ethylene-glycol ($\rho = 1.1 \times 10^3$ kg/m^3, $\gamma = 4.5 \times 10^{-2}$ N/m, and $\nu = 7.6 \times 10^{-6}$ m^2/s) and the experimental parameters are $R_c = 3.8 \times 10^{-2}$ m, $h_c = 2.76 \times 10^{-3}$ m, and $Q_0 = 27 \times 10^{-6}$ m^3/s. These parameters give the dimensionless numbers $\epsilon = 7.2 \times 10^{-2}$, $\mathrm{Re} = 2.2$, $G = 8.7$, and $B = 2.5 \times 10^{-2}$ (see text).

It is noteworthy how our solution reproduces the eddy observed in Refs. [7,9] that helps to slow down the velocity and increases the height of the fluid (see Fig. 1). Moreover, our numerical simulations show a slow dependence of r_j with the height h_c, but a strong dependence on the value of the flux Q_0. This is also consistent with the experimental observations made by Hansen *et al.* [9] and the scaling proposed in [7,15]

A more systematic analysis of our solutions is made in Fig. 2 where we compare the experiments in Ref. [9] with the value of the jump radius given by our numerical simulations. There is a very good agreement between the model and experiments except for small values of Q_0 and high viscosity. This is explained in the insets of Fig. 2 by observing that the jump is spread over a wider region under these conditions. As noted in [9] the radius of the jump for low viscosity is difficult to define experimentally and we expect differences between our numerical definition and their experimental optical method.

A second application of Eqs. (8) is the study of Faraday instability for a thin layer of fluid of height h. The acceleration of the supporting plate is equivalent to having an effective gravity that depends on time. For a sinusoidal acceleration with a single frequency forcing this means $g(t) = g[1 + \Gamma \cos\Omega t]$ or $G(t) = G[1 + \Gamma \cos t]$ in dimensionless variables. Here $\Gamma = a/g$ is the ratio of the forcing acceleration a to the gravitational one. The horizontal length scale L can be reabsorbed in the horizontal derivatives of Eqs. (8) reflecting the fact that it can be chosen by the system itself. To fix our scale L in the horizontal direction, we measure the lengths in units of h. Thus, we take $L = h$ in our equations [16]. The definitions of Re, G, and B are straightforward.

The linearization of Eqs. (8) gives the Mathieu equation predicted in [12] at first order in ϵ^2

$$\frac{6}{5}\mathrm{Re}\partial_t^2\xi + \left(3 - \frac{27}{5}\nabla_\perp^2\right)\partial_t\xi - [G(t) - B\nabla_\perp^2]\nabla_\perp^2\xi = 0. \quad (10)$$

Thus, our equations are linearly unstable for a sufficiently high forcing and can predict the critical acceleration and wave number observed at the onset of instability [12,17]. Figure 3 shows the critical acceleration obtained from Eq. (10) compared to the experiments of Wagner *et al.* [18] for low values of Reynolds number ($\mathrm{Re} < 4.6$) and near a bicritical point where harmonic and subharmonic waves are observed. We also show in supplementary ma-

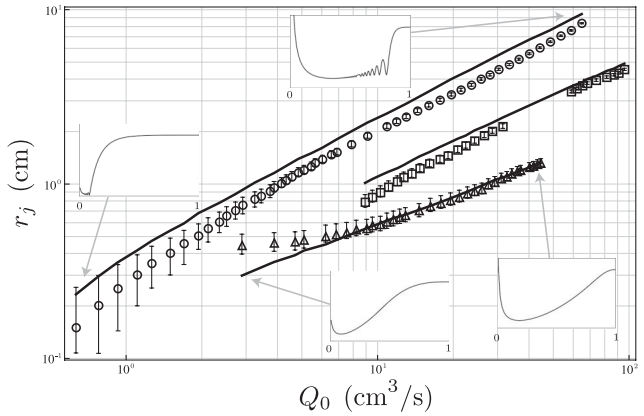

FIG. 2. Radius of the jump position as function of the flow rate for three liquids with different relative viscosities $\tilde{\nu} = \nu/\nu_{\text{water}}$. The symbols, including the error bars, represent experimental measures extracted from Ref. [9] for water (squares, $\tilde{\nu} = 1$, $\rho = 1.0 \times 10^3$ kg/m^3, $\gamma = 7.4 \times 10^{-2}$ N/m, $R_c = 2 \times 10^{-1}$ m, $h_c = 1.5 \times 10^{-3}$ m), oil (triangles, $\tilde{\nu} = 15$, $R_c = 1.7 \times 10^{-1}$ m, $h_c = 1.5 \times 10^{-3}$ m) and a much more viscous oil (circles, $\tilde{\nu} = 95$, $R_c = 1.7 \times 10^{-1}$ m, $h_c = 1.5 \times 10^{-3}$ m) [19]. The solid curves are the prediction for the jump radii obtained from Eq. (9). Insets: numerical profiles of the fluid surface in dimensionless coordinates for different values of fluid flow and viscosity.

terial that Eqs. (8) can saturate the instability by numerically computing the solutions of (8) on a staggered spatial mesh. (See supplementary material [14] for a detailed description of our numerical simulations and comparison with experiments.)

We close our discussion by pointing out that Eqs. (8) represents the minimal form of a formal expansion in two parameters Re and ϵ^2. Inertial terms in the NS equations and nonlinearities in the boundary conditions are described at the lowest order allowing the use of Eqs. (8) in different situations. Here we have explored the circular hydraulic jump and Faraday instability in very simple situations, but our analysis could be modified to study hydraulic jumps in nonaxisymmetric cases and planar geometries, Faraday instability with different types of forcing and boundary conditions, or any other physical situation in which inertial terms play a fundamental role in understanding the dynamics of a shallow viscous layer of fluid.

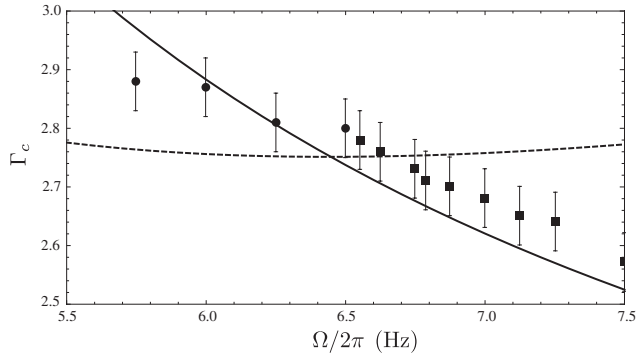

FIG. 3. Critical acceleration Γ as a function of the driving frequency $\Omega/2\pi$ for a silicon oil layer ($h = 7 \times 10^{-4}$ m, $\nu = 5 \times 10^{-6}$ m^2/s, $\gamma = 1.94 \times 10^{-2}$ N/m, and $\rho = 9.2 \times 10^2$ kg/m^3). The circles and squares (with error bars) mark the experimental values of Ref. [18] for the harmonic and the subharmonic responses, respectively. The black line shows the threshold for subharmonic waves obtained from Eq. (10). Similarly, the dotted line gives the threshold for harmonic waves. At a critical frequency $\Omega/2\pi \approx 6.5$ both lines intersect marking a bicritical point.

N. R. is grateful for the financial support of CONICYT. E. C. and E. T. acknowledge the support of Anillo Act No. 15. E. C. thanks Fondecyt Project No. 1095112. Simulations were done using the XDIM Software developed by M. Monticelli and P. Coullet.

[1] L. D. Landau and E. M. Lifshitz, *Fluid Mechanics* (Pergamon, Oxford, 1987).
[2] D. J. Acheson, *Elementary Fluid Dynamics* (Oxford University Press, Oxford, 2003).
[3] J. W. Strutt, *Theory of Sound* (Dover, New York, 1945), Vol 2.
[4] P. D. Howell, Eur. J. Appl. Math. **7**, 321 (1996).
[5] J. A. Teichman, Ph.D. thesis, MIT, 2002.
[6] A. Oron, S. H. Davis, and S. G. Bankoff, Rev. Mod. Phys. **69**, 931 (1997).
[7] T. Bohr, V. Putkaradze, and S. Watanabe, Phys. Rev. Lett. **79**, 1038 (1997); S. Watanabe, V. Putkaradze, and T. Bohr, J. Fluid Mech. **480**, 233 (2003); T. Bohr, C. Ellegaard, A. E. Hansen, and A. Haaning, Physica (Amsterdam) **228B** , 1 (1996).
[8] J. W. M. Bush, J. M. Aristoff, and A. E. Hosoi, J. Fluid Mech. **558**, 33 (2006).
[9] S. T. Hansen, S. Horlück, D. Zauner, P. Dimon, C. Ellegaard, and S. C. Creagh, Phys. Rev. E **55**, 7048 (1997).
[10] T. B. Benjamin and F. Ursell, Proc. R. Soc. A **225**, 505 (1954); M. Faraday, Phil. Trans. R. Soc. London **121**, 299 (1831).
[11] K. Kumar, Proc. R. Soc. A **452**, 1113 (1996).
[12] E. Cerda and E. Tirapegui, J. Fluid Mech. **368**, 195 (1998).
[13] W. S. Edwards and S. Fauve, Phys. Rev. E **47**, R788 (1993).
[14] See supplementary material at http://link.aps.org/supplemental/10.1103/PhysRevLett.104.187801.
[15] Our equations are different than the ones used by Bohr *et al.* [7] and we are still working to understand the connection of their work with our expansion.
[16] The natural horizontal length scale is the wavelength λ of the instability; however, this length is known *a posteriori*. By taking $\epsilon = 1$ we expect that the horizontal derivatives are of order $\mathcal{O}(\nabla_\perp) \sim h/\lambda \ll 1$.
[17] F. Mancebo and J. Vega, J. Fluid Mech. **467**, 307 (2002).
[18] C. Wagner, H. W. Müller, and K. Knorr, Phys. Rev. E **68**, 066204 (2003).
[19] The density and surface tension of both oils are not given in [9]. We use the standard values $\rho = 9.5 \times 10^2$ kg/m^3 and $\gamma = 2.0 \times 10^{-2}$ N/m in our fit.